PNAS RESEARCH ARTICLE | PHYSICS OPEN ACCESS

Phonon screening and dissociation of excitons at finite temperatures from first principles

Antonios M. Alvertis[a,b], Jonah B. Haber[b,c], Zhenglu Li[b,d,e], Christopher J. N. Coveney[f], Steven G. Louie[b,e], Marina R. Filip[f], and Jeffrey B. Neaton[b,e,g,1]

Affiliations are included on p. 11.

Edited by Angel Rubio, Max-Planck-Institut fur Struktur und Dynamik der Materie, Hamburg, Germany; received February 19, 2024; accepted June 11, 2024

The properties of excitons, or correlated electron–hole pairs, are of paramount importance to optoelectronic applications of materials. A central component of exciton physics is the electron–hole interaction, which is commonly treated as screened solely by electrons within a material. However, nuclear motion can screen this Coulomb interaction as well, with several recent studies developing model approaches for approximating the phonon screening of excitonic properties. While these model approaches tend to improve agreement with experiment, they rely on several approximations that restrict their applicability to a wide range of materials, and thus far they have neglected the effect of finite temperatures. Here, we develop a fully first-principles, parameter-free approach to compute the temperature-dependent effects of phonon screening within the ab initio *GW*-Bethe–Salpeter equation framework. We recover previously proposed models of phonon screening as well-defined limits of our general framework, and discuss their validity by comparing them against our first-principles results. We develop an efficient computational workflow and apply it to a diverse set of semiconductors, specifically AlN, CdS, GaN, MgO, and $SrTiO_3$. We demonstrate under different physical scenarios how excitons may be screened by multiple polar optical or acoustic phonons, how their binding energies can exhibit strong temperature dependence, and the ultrafast timescales on which they dissociate into free electron–hole pairs.

excitons | phonons | phonon screening | Bethe–Salpeter equation

Significance

Excitons, or correlated electron-hole pairs, are prevalent in condensed matter and crucial to optoelectronic function of materials. First-principles calculations now predict excitonic effects in increasingly complex systems, including exciton-phonon interactions and dynamics. While the electronic screening of the Coulomb interaction binding excitons is critical to determining their properties, phonon screening has been typically neglected and, when accounted for, it is treated with simplified models. Here we debut a general ab initio framework that captures both electron and phonon screening of excitons in materials. We demonstrate that phonon screening can dramatically alter predicted exciton properties, leading to strongly temperature-dependent binding energies and ultrafast dissociation, paving the way for the discovery of new exciton physics in complex materials.

Excitons, correlated electron–hole pairs often generated upon photoexcitation, are critical to semiconductor optoelectronic applications. The dissociation of bound excitons into free charge carriers is central to photovoltaics (1, 2), while their ability to recombine and emit light underpins applications such as light-emitting diodes (3, 4). Capturing the materials-specific many-body interactions of electrons and holes in solids requires careful theoretical descriptions of screening and scattering mechanisms, and constitutes a major challenge for first-principles approaches. The state-of-the-art ab initio framework to describe excitons within many-body perturbation theory is based on the *GW* approximation (5, 6) and Bethe–Salpeter equation (BSE) (7–10) (*GW*+BSE), where G is the one-particle Green's function and W is the screened Coulomb interaction. A key ingredient responsible for the formation of bound excitons is the frequency-dependent (ω) screened Coulomb interaction (9–11)

$$W(\mathbf{r}, \mathbf{r}', \omega) = \int d\mathbf{r}'' \epsilon^{-1}(\mathbf{r}, \mathbf{r}'', \omega) v(\mathbf{r}'', \mathbf{r}'), \quad [1]$$

where v is the bare Coulomb interaction and $\epsilon(\mathbf{r}, \mathbf{r}'', \omega)$ is the frequency-dependent, nonlocal dielectric function. Most commonly, ϵ is obtained within the random-phase approximation (RPA) (12) and describes screening only originating from the perturbation of the electron density in the limit of clamped ions, the electronic screening.

However, exciton binding energies computed within the standard ab initio *GW*+BSE framework can overestimate experiments, by up to a factor of three in certain heteropolar crystals (13), a discrepancy attributed to the screening of Coulomb interactions due to polar ionic vibrations (13–18), normally neglected in standard approaches. The phonon contribution to the low-frequency (static) dielectric constant, ϵ_0, in addition to the high-frequency (optical) counterpart, ϵ_∞, sets the scale of the screening originating from ionic vibrations, namely $\epsilon_o - \epsilon_\infty$. This raises the question of which dielectric constant more appropriately describes the screening of weakly interacting electrons and holes (i.e., with a binding energy comparable to phonon energies), with several studies

Author contributions: M.R.F. and J.B.N. designed research; A.M.A., J.B.H., Z.L., and C.J.N.C. performed research; A.M.A., J.B.H., S.G.L., M.R.F., and J.B.N. analyzed data; S.G.L. provided guidance; and A.M.A., J.B.H., Z.L., C.J.N.C., S.G.L., M.R.F., and J.B.N. wrote the paper.

The authors declare no competing interest.

This article is a PNAS Direct Submission.

[1]To whom correspondence may be addressed. Email: jbneaton@lbl.gov.

This article contains supporting information online at https://www.pnas.org/lookup/suppl/doi:10.1073/pnas.2403434121/-/DCSupplemental.

Published July 18, 2024.

proposing an intermediate ad hoc "effective" dielectric constant with a value between these two limits ϵ_o and ϵ_∞ (19–21), in an effort to account for screening from both electrons and phonons and to capture experimental trends. An alternative approach is to modify the dielectric function of Eq. **1** so that it includes the contributions from polar phonons (15, 22). Several model approaches have been reported that include phonon contributions W^{ph} to the screened Coulomb interaction to complement the standard clamped-ion electronic screening $W = W^{el}$ (19, 23–25). The results from such approaches can vary significantly depending on approximations that are used; they are limited to the description of screening from polar zone-center phonons; and they do not yield detailed microscopic insights into these effects relative to electronic screening. A rigorous, fully first-principles, description of both electronic and phonon screening of excitons on equal footing is therefore necessary to develop truly predictive accuracy for exciton properties in diverse materials, and to reach a deeper understanding of factors affecting the relative importance and interplay of these two effects.

Within many-body perturbation theory and to the lowest order in the electron–phonon interaction, the lattice contribution to the screened Coulomb interaction is given by (26–28)

$$W^{ph}(\mathbf{r}, \mathbf{r}', \omega) = \sum_{\mathbf{q},\nu} D_{\mathbf{q},\nu}(\omega) g_{\mathbf{q},\nu}(\mathbf{r}) g^*_{\mathbf{q},\nu}(\mathbf{r}'), \qquad [2]$$

where $D_{\mathbf{q},\nu}(\omega)$ is the propagator of a phonon with branch index ν at wavevector $\mathbf{q}$, and $g_{\mathbf{q},\nu}$ is the electron–phonon vertex. We refer to Eq. **2** as the phonon-screened Coulomb interaction, as the screening in this term arises from phonons. Ref. 25 used this expression to derive a 0 K correction to the electron–hole interaction term in the ab initio BSE due to phonon screening, subsequently approximating it for "hydrogenic" excitons and long range polar electron–phonon interactions described by the Fröhlich model. For a number of systems where these approximations are well justified, this notably improved agreement with experiment for exciton binding energies.

Here, we generalize the approach in ref. 25 to finite temperatures and implement it within a fully ab initio BSE framework, accounting for the effects of phonon screening to lowest order in the electron–phonon interaction, at the level of phonon exchange. Ref. 25 is one of several recent papers (14, 22) that, building on pioneering work of Hedin and Lundqvist (29) and Strinati (11) decades earlier, include the effects of phonon screening on exciton properties, within ab initio many-body perturbation theory. Closely related recent works treat general exciton–phonon interactions in a modern first-principles context, and using cumulants (30), using two-particle Green's functions (31) and using a linear-response real-time framework (32), have derived phonon-renormalized exciton properties in terms of the exciton–phonon vertex, analogous to the one used in the seminal work of Toyozawa (33). Some recent ab initio calculations of exciton–phonon interactions in solids capture phenomena such as phonon-assisted absorption and luminescence (34–36), temperature-dependent exciton localization (37) and shifts of the exciton energy (38), and report exciton–exciton scattering rates (39–41). However, a fully first-principles framework for capturing finite temperature dynamical screening of excitons due to phonons, and the impact of these effects on the binding energy and dynamics of excitons, is thus far missing. Here, starting from Eq. **2**, we develop and implement a temperature-dependent complex correction to the standard clamped-ion BSE kernel, referred to in what follows as the phonon kernel, K_{ph}, that captures dynamical phonon screening to lowest order. Although it is possible to recover or go beyond the exciton–phonon self-energy of ref. 31 starting from W_{ph} by including other higher-order diagrams in the BSE (30), here we retain only the phonon exchange diagram of ref. 31 (equivalently Eq. **2**), a judicious, computationally efficient, and physical low-order approximation for semiconductor systems (ref. 24) that rigorously includes phonon screening and for which free electron- and hole-polaron radii (as described by Fan-Migdal diagrams) are on the same order as exciton radii (19, 42). As we show in what follows, within the limits of perturbation theory, the real part of K_{ph} in the exciton basis provides a quantitative prediction of the temperature-dependent renormalization of exciton (binding) energies via phonon screening and the imaginary part can lead to a quantitative rate of dissociation of an exciton into free electron and holes through absorption of a phonon within the approximations made here.

Computing the temperature-dependent effect of phonon screening on excitons in a select set of semiconductors, we predict that phonons are responsible for a 50% reduction of the exciton binding energy of CdS at room temperature, with acoustic phonons having a substantial contribution. Moreover, we predict that phonon absorption by excitons in GaN contribute to their ultrafast dissociation into free charge carriers with a timescale that is consistent with experimental measurements for similar materials. In $SrTiO_3$, we find multiple polar phonons can contribute to the screening of excitons at once, leading to a significant overall reduction of the exciton binding energy. Finally, we show how approximations to our first-principles results lead to models that are commonly used in the literature, such as the Haken potential (23, 24), and we discuss the validity of these models for different systems.

The structure of this paper is as follows. We first present the theoretical background of our work and summarize the derivation of the first-principles phonon screening correction to the BSE kernel at finite temperatures, discussing both the real and imaginary parts of this kernel, and the observables that may be extracted from these quantities. We then examine different approximations to this phonon kernel, and connect our work to model results from the literature. We then proceed to present the bulk of our computational results. Specifically, we start by presenting our first-principles results at 0 K for a range of systems, and compare these to the predictions of various models of phonon screening, also discussing the origin of observed differences. We then present an in-depth application of our ab initio workflow to selected materials and their temperature-dependent phonon screening and exciton dissociation properties. Finally, we provide a discussion and outlook for our work.

First-Principles Phonon Kernel

The BSE within the Tamm–Dancoff approximation for zero-momentum excitons in reciprocal space is written as (10)

$$(E_{c\mathbf{k}} - E_{v\mathbf{k}}) A^S_{cv\mathbf{k}} + \sum_{c'v'\mathbf{k}'} \langle cv\mathbf{k}|K^{eh}|c'v'\mathbf{k}'\rangle A^S_{c'v'\mathbf{k}'} = \Omega^S A^S_{cv\mathbf{k}}, \qquad [3]$$

where $E_{c\mathbf{k}}$ and $E_{v\mathbf{k}}$ are the quasiparticle energies of conduction and valence bands, respectively. The BSE of Eq. **3** describes excited states accounting only for electronic screening effects, and will hence be referred to as the "bare" BSE, to distinguish it from

the case where phonon screening is included. The coefficients $A^S_{cv\mathbf{k}}$ describe the corresponding excited state S with excitation energy Ω_S as a linear combination of free electron–hole pair wave functions [$|cv\mathbf{k}\rangle$, typically obtained from a density functional theory (DFT) calculation], namely

$$|S\rangle = \sum_{cv\mathbf{k}} A^S_{cv\mathbf{k}} |cv\mathbf{k}\rangle. \quad [4]$$

The kernel K^{eh} describes the interaction between electrons and holes and consists of direct (d) and exchange (x) contributions, $K^{eh} = K^d + K^x$. The repulsive exchange term K^x depends on the bare Coulomb interactions and is frequency-independent. In the absence of spin–orbit coupling, this term is only nonzero for excitons of zero spin, and is responsible for the different properties of singlet and triplet excitons (10). On the other hand, the direct term is attractive, frequency-dependent, and involves the screened Coulomb interaction W. This term can be written as

$$K^d_{cv\mathbf{k},c'v'\mathbf{k}'}(\Omega) = -\left\langle cv\mathbf{k} \left| \frac{i}{2\pi} \int d\omega e^{-i\omega\delta} W(\mathbf{r}, \mathbf{r}', \omega) \times \left[\frac{1}{\Omega - \omega - \Delta_{c'\mathbf{k}'v\mathbf{k}} + i\delta} + \frac{1}{\Omega + \omega - \Delta_{c\mathbf{k}v'\mathbf{k}'} + i\delta} \right] \right| c'v'\mathbf{k}' \right\rangle, \quad [5]$$

where δ is a small real and positive number and we have introduced the notation $\Delta_{c\mathbf{k}v\mathbf{k}} = E_{c\mathbf{k}} - E_{v\mathbf{k}}$. This kernel term is usually computed in the clamped-ion limit including only electronic screening, i.e., $W = W^{el}$ (9, 10). While W^{el} is fully frequency-dependent in principle, since exciton binding energies are much smaller than the band gaps and the plasmon energies in many insulators, the dynamical properties of W^{el} are often neglected for weakly bound excitons (10), namely $K^{el}_{cv\mathbf{k},c'v'\mathbf{k}'}(\Omega_S) = \langle cv\mathbf{k}|W^{el}(\mathbf{r}, \mathbf{r}', \omega = 0)|c'v'\mathbf{k}'\rangle$. Dynamical effects can be important in some cases, for example in order to account for free carrier screening from acoustic plasmons (43–45).

We now include the contribution of phonon screening to the kernel, taking $W = W^{el} + W^{ph}$, which will yield a correction K^{ph} to the direct kernel of Eq. **5**. To obtain this phonon kernel K^{ph}, we introduce the phonon screening of Eq. **2** into Eq. **5**, with the phonon propagator appearing in Eq. **2** written as (46)

$$D_{\mathbf{q},\nu}(\omega) = \frac{1}{\omega - \omega_{\mathbf{q},\nu} + i\delta} - \frac{1}{\omega + \omega_{\mathbf{q},\nu} - i\delta}. \quad [6]$$

Therefore, as in ref. 25, we arrive to the following expression for the phonon kernel

$$K^{ph}_{cv\mathbf{k},c'v'\mathbf{k}'}(\Omega) = -\sum_{\mathbf{q},\nu} g_{cc'\nu}(\mathbf{k}', \mathbf{q}) g^*_{vv'\nu}(\mathbf{k}', \mathbf{q}) \times \left[\frac{1}{\Omega - \Delta_{c\mathbf{k}v'\mathbf{k}'} - \omega_{\mathbf{q},\nu} + i\eta} + \frac{1}{\Omega - \Delta_{c'\mathbf{k}'v\mathbf{k}} - \omega_{\mathbf{q},\nu} + i\eta} \right], \quad [7]$$

where η is a small real and positive number. Here, $\mathbf{q} = \mathbf{k} - \mathbf{k}'$ and $g_{nm\nu}(\mathbf{k}', \mathbf{q}) = \langle n\mathbf{k}' + \mathbf{q}|g_{\mathbf{q}\nu}|m\mathbf{k}'\rangle$, which can be computed, for example, via density functional perturbation theory (DFPT) (47) or beyond, via GW perturbation theory (GWPT) (48).

The result of Eq. **7** is only valid at zero temperature. We extend the phonon kernel to finite temperatures via the Matsubara formalism. Here, the integral of Eq. **5** is analytically continued into the complex plane and evaluated at imaginary bosonic Matsubara frequencies. Following this well-established procedure (46), we obtain the following expression for the temperature-dependent phonon contribution to the kernel

$$K^{ph}_{cv\mathbf{k},c'v'\mathbf{k}'}(\Omega, T) = -\sum_{\mathbf{q},\nu} g_{cc'\nu}(\mathbf{k}', \mathbf{q}) g^*_{vv'\nu}(\mathbf{k}', \mathbf{q}) \times \left[\frac{N_B(\omega_{\mathbf{q},\nu}, T) + 1 + N_B(\Delta_{c\mathbf{k}v'\mathbf{k}'}, T)}{\Omega - \Delta_{c\mathbf{k}v'\mathbf{k}'} - \omega_{\mathbf{q},\nu} + i\eta} + \frac{N_B(\omega_{\mathbf{q},\nu}, T) + 1 + N_B(\Delta_{c'\mathbf{k}'v\mathbf{k}}, T)}{\Omega - \Delta_{c'\mathbf{k}'v\mathbf{k}} - \omega_{\mathbf{q},\nu} + i\eta} + \frac{N_B(\omega_{\mathbf{q},\nu}, T) - N_B(\Delta_{c\mathbf{k}v'\mathbf{k}'}, T)}{\Omega - \Delta_{c\mathbf{k}v'\mathbf{k}'} + \omega_{\mathbf{q},\nu} + i\eta} + \frac{N_B(\omega_{\mathbf{q},\nu}, T) - N_B(\Delta_{c'\mathbf{k}'v\mathbf{k}}, T)}{\Omega - \Delta_{c'\mathbf{k}'v\mathbf{k}} + \omega_{\mathbf{q},\nu} + i\eta} \right], \quad [8]$$

where N_B is the Bose–Einstein occupation factor at temperature T. A detailed derivation of Eq. **8** is given in *SI Appendix*, section S3. As we are concerned with temperatures near room temperature and materials with band gaps that are large compared to phonon energies, we use the fact that $N_B(\Delta_{c\mathbf{k}v\mathbf{k}}, T) \ll N_B(\omega_{\mathbf{q},\nu}, T)$ moving forward.

The first two terms within the bracket of Eq. **8** describe the contribution of phonon emission to the kernel, and these terms are finite even at 0 K. The last two terms within the bracket of Eq. **8** are due to the absorption of phonons, and are only nonzero at temperatures greater than zero. In this work, we implement the ab initio phonon kernel (as a matrix) rewritten in the bare or unperturbed exciton basis as

$$K^{ph}_{S,S'}(\Omega, T) = -\sum_{cv\mathbf{k}c'v'\mathbf{k}'\nu} A^{S*}_{cv\mathbf{k}} g_{cc'\nu}(\mathbf{k}', \mathbf{q}) g^*_{vv'\nu}(\mathbf{k}', \mathbf{q}) A^{S'}_{c'v'\mathbf{k}'} \times \left[\frac{N_B(\omega_{\mathbf{q},\nu}, T) + 1}{\Omega - \Delta_{c\mathbf{k}v'\mathbf{k}'} - \omega_{\mathbf{q},\nu} + i\eta} + \frac{N_B(\omega_{\mathbf{q},\nu}, T) + 1}{\Omega - \Delta_{c'\mathbf{k}'v\mathbf{k}} - \omega_{\mathbf{q},\nu} + i\eta} + \frac{N_B(\omega_{\mathbf{q},\nu}, T)}{\Omega - \Delta_{c\mathbf{k}v'\mathbf{k}'} + \omega_{\mathbf{q},\nu} + i\eta} + \frac{N_B(\omega_{\mathbf{q},\nu}, T)}{\Omega - \Delta_{c'\mathbf{k}'v\mathbf{k}} + \omega_{\mathbf{q},\nu} + i\eta} \right], \quad [9]$$

where the off-diagonal matrix elements of $K^{ph}_{S,S'}$ describe the extent to which the exciton–phonon scattering significantly changes the character of the excited state S. It should also be noted that since here we work within many-body perturbation theory, this scheme might lead to poorer descriptions of system with strong nonperturbative electron–phonon coupling. Moreover, multiphonon processes, which are not captured here, can become significant near room temperature for certain systems (49).

Converging phonon screening properties requires the sum of Eq. **9** to be computed on a dense grid in reciprocal space. Wannier-Fourier interpolation can be utilized to facilitate the calculation of electron–phonon matrix elements g on a dense grid, by interpolating their values obtained via DFPT on a

coarse grid (50). However, Wannier interpolation introduces an additional phase factor to the electron–phonon matrix elements, which is not present in the wavefunctions used to compute the BSE kernel on a fine grid. This inevitably leads to a gauge inconsistency between the values of g and the exciton coefficients, and for this reason, it has not so far been possible to take advantage of Wannier-based techniques to compute exciton–phonon interactions from first-principles, restricting previous calculations to a limited number of systems with exciton properties that are converged with relatively coarse k-grid samplings (39, 40, 51, 52). Yet the vast majority of bulk semiconductors require an ultrafine sampling of the Brillouin zone to obtain converged exciton properties (53), which consequently necessitates an ultradense sampling for capturing their exciton–phonon interactions. It is therefore imperative to employ Wannier interpolation techniques to obtain meaningful results on the exciton–phonon interactions of general bulk semiconductors, making the gauge inconsistency that these introduce one of the main limiting factors toward this goal. To address this challenge, we use the strategy of computing the exact same set of Wannier-interpolated wavefunctions from DFT on a fine k-grid, and use their plane-wave basis representation to perform BSE calculations with the BerkeleyGW code (54), and their Wannier basis representation to obtain electron–phonon matrix elements on the same fine k-grid from DFPT using the EPW code (55). Consequently, the gauge consistency is naturally guaranteed. This functionality is included in the wannier2bgw.py utility of the BerkeleyGW code, which will also be the subject of a separate work. Additional discussion on this issue is provided in *SI Appendix*, section S1. Our work combines Wannier interpolation methods for electron-phonon and electron-hole interactions from first principles, hence not only greatly accelerating our calculations, but also giving us access to the study of systems such as $SrTiO_3$ and the nitrides GaN and AlN, which would otherwise be computationally prohibitive.

Overall, inclusion of phonon screening in Eq. **3** leads to the following generalized BSE

$$(E_{c\mathbf{k}} - E_{v\mathbf{k}})A^{S,ph}_{cv\mathbf{k}} + \sum_{c'v'\mathbf{k}'} \langle cv\mathbf{k}|K^{eh} + K^{ph}(\omega, T)|c'v'\mathbf{k}'\rangle A^{S,ph}_{c'v'\mathbf{k}'} = \Omega^{S,ph}A^{S,ph}_{cv\mathbf{k}}. \quad [10]$$

The superscript in the eigenvalues and eigenvectors $\Omega^{S,ph}$, $A^{S,ph}$ highlights that the excited states S arising from the solution of Eq. **10** now include the effect of phonon screening. While one can diagonalize the combined kernel $K = K^{eh} + K^{ph}$ to find the solutions of Eq. **10**, for the systems considered in this work it is an excellent approximation to consider the effect of phonon screening as a small perturbation. We will therefore obtain the effect of phonon screening on excited states within first-order perturbation theory in this work, as discussed in the following Section.

Real Part of the Phonon Kernel. For nondegenerate excitons of energy Ω_S, the correction to their energies from phonon screening within first-order perturbation theory is

$$\Delta\Omega_S = \mathrm{Re}\left[\langle S|K^{ph}(\Omega_S)|S\rangle\right]. \quad [11]$$

For a subspace of degenerate excitons with dimension N_S, the phonon screening correction to the exciton energies is taken to be equal to the normalized trace of the $N_S \times N_S$ K^{ph} matrix, calculated as $\Delta\Omega_S = \frac{1}{N_S}\mathrm{Tr}[K^{ph}(\Omega_S)]$, which is gauge-invariant. More rigorously, corrections to the exciton energy due to phonon screening at the level of Eq. **2** require a sum over several exciton states; however, here we find these corrections to be unimportant, since these are proportional to the off-diagonal matrix elements of $K^{ph}_{S,S'}$, which for the systems studied here are of the order of 10^{-3} to 10^{-2} meV. In *SI Appendix*, section S10, we demonstrate the convergence of phonon screening with the number of excited states included in the phonon kernel for two of the studied materials, CdS and MgO. When considering a sum over hundreds of exciton states, the second-order correction to the exciton binding energy was found to be smaller than 0.1 meV, and can therefore be safely neglected. For the same reason, first-order corrections to exciton wavefunctions are negligible for the systems studied here, and we therefore focus in what follows on computing the correction of Eq. **11** to the exciton energies.

We note here that in principle the effect of phonon screening could also be included in the GW self-energy, yielding a correction iGW^{ph} to the quasiparticle band structure, and $E_{c\mathbf{k}}$, $E_{v\mathbf{k}}$ in Eq. **10**. This frequency- and temperature-dependent correction is equivalent to the one described by the so-called Fan-Migdal self-energy (30), Σ^{FM}, the real part of which captures low-order energy renormalization and mass enhancement due to electron–phonon interactions (50). Therefore, if one were to include the effect of phonon screening both in the GW self-energy and in the BSE kernel this would generalize the BSE of Eq. **10** so that the bare electron and hole energies are substituted by the respective polaron energies $\tilde{E}_{c\mathbf{k}} = E_{c\mathbf{k}} + \Sigma^{FM}_c(\omega, T)$ and $\tilde{E}_{v\mathbf{k}} = E_{v\mathbf{k}} + \Sigma^{FM}_v(\omega, T)$. Ref. 56 included such a temperature dependence for the quasiparticle energies, but did not account for the contribution of phonon screening to excitons.

The exciton–phonon interaction was described in ref. 31 as the sum of three distinct contributions to the self-energy: the dynamical Fan-Migdal term, the dynamical phonon exchange term, and the frequency-independent Debye-Waller term. An equivalent self-energy for the exciton was derived in ref. 30 within a cumulant approach. We note that the phonon exchange term in ref. 31 is equivalent to Eq. **8** and that the Debye-Waller term does not affect the exciton binding energy. Thus, inclusion of the phonon kernel and the Fan-Migdal term in the BSE would be, strictly speaking, consistent with ref. 31. Our approach is distinct from that of ref. 32, which presented an alternative derivation of the exciton–phonon self-energy, based on a BSE in which an optical response function is defined as the variation of the electronic density with respect to the total potential (rather than only the external potential, as in ref. 31); the use of this alternative approach was reported to lead to small differences in computed exciton linewidths for monolayer MoS_2 and $MoSe_2$ (32). While a deeper comparison of the distinct approaches of refs. 31 and 32 is reserved for future work, we expect that, quantitatively, changes to the exciton–phonon interaction originating from different formulations of the BSE will be small compared with the effects of phonon screening, given our ab initio results presented below, and the results in ref. 32. Moreover, we note that the exciton–phonon self-energy of ref. 32 also contains a phonon exchange diagram that is equivalent to that of ref. 31 and central to our work here, which focuses on phonon screening.

The Fan-Migdal term of the exciton–phonon self-energy physically describes the induced lattice polarization around the exciton's constituent electron and hole as if the two particles were independent, i.e., it describes the formation of an independent electron-polaron and hole-polaron, without accounting for any

modifications of the lattice polarization when the electron and hole are bound together. However, as noted recently in refs. 57 and 58, the formation of an exciton results in at least a partial cancelation of the lattice distortion associated with the independent electron- and hole-polarons, due to the mutual Coulomb attraction of these leading to a cancelation of the electron and hole charge densities. This picture is in agreement with what was noted originally in refs. 19 and 42 and reiterated recently in ref. 25, that is that the lattice polarization associated with the polarons may interfere significantly, and even possibly cancel each other. This so-called polaronic interference effect was described in ref. 19 and subsequently in ref. 42 through a higher-order phonon vertex correction to the exciton binding energy, in addition to the Fan–Migdal and phonon exchange contributions. Moreover, ref. 19 reported that depending on the relative exciton and electron (hole) polaron radii, this term can partly, or in some cases even completely, cancel out with the Fan-Migdal term, as expected from the intuitive picture discussed above and also found in refs. 57 and 58. This cancelation of the Fan-Migdal term with higher-order exciton–phonon vertex corrections is reminiscent of an analogous cancelation that has been reported in the electronic case (59).

Therefore, in the absence of including polaronic interference effects through higher-order corrections, neglecting the Fan-Migdal term of the exciton–phonon self-energy (31, 32) in constructing K_{ph} is an acceptable approximation here, particularly given the focus on phonon screening. Indeed, for several semiconductors, including those studied in this work, exciton and electron (hole) polaron radii have similar estimated values (*SI Appendix*, section S2), strongly suggesting that naive inclusion of the Fan-Migdal term at lowest order while ignoring interference effects that enter at higher order will lead to significant errors. We therefore restrict our focus to phonon exchange and phonon screening, and reserve a more rigorous treatment of polaronic mass enhancement and interference effects (19, 42) for future work. Thus, in what follows, the phonon screening shift of the lowest bound exciton energy, $\Delta\Omega_S$, as obtained through Eq. **11**, is given by the reduction of the exciton binding energy of the same magnitude, i.e., $\Delta E_B = -\Delta\Omega_S$.

Imaginary Part of the Phonon Kernel. The phonon kernel of Eq. **9** is a complex quantity. For phonon emission and for $\omega = \Omega_S$, the imaginary part of the phonon kernel is proportional to

$$\delta[\Omega_S - \omega_{\mathbf{q},\nu} - (E_{c\mathbf{k}'} - E_{v\mathbf{k}})] + \delta[\Omega_S - \omega_{\mathbf{q},\nu} - (E_{c\mathbf{k}} - E_{v\mathbf{k}'})], \quad [12]$$

while for absorption it is proportional to

$$\delta[\Omega_S + \omega_{\mathbf{q},\nu} - (E_{c\mathbf{k}'} - E_{v\mathbf{k}})] + \delta[\Omega_S + \omega_{\mathbf{q},\nu} - (E_{c\mathbf{k}} - E_{v\mathbf{k}'})]. \quad [13]$$

For excitons of zero momentum, the conservation of energy condition, $\Omega_S - \omega_{\mathbf{q},\nu} = E_{c\mathbf{k}'} - E_{v\mathbf{k}}$, which must be met for the emission channel to make nonzero contributions to the imaginary part of the phonon kernel, may only be satisfied for so-called "resonant" excitons with energies greater than the quasiparticle band gap. This could occur for indirect band gap materials with resonant excitons above the fundamental gap, e.g., silver-pnictogen halide double perovskites (60). Alternatively, this condition may be satisfied for higher-lying exciton states in the continuum, the analysis of which is beyond the scope of the present study. On the other hand, phonon absorption, $\Omega_S + \omega_{\mathbf{q},\nu} = E_{c\mathbf{k}'} - E_{v\mathbf{k}}$, can occur if the energy of an exciton which has absorbed a phonon matches that of a free electron–hole pair, as schematically depicted in Fig. 1 for the example of a LO phonon with frequency ω_{LO}. Specifically, this condition is only satisfied in a single-phonon process if the absorbed phonon has a greater or equal frequency than the exciton binding energy, i.e., $\omega_{\mathbf{q},\nu} \geq E_B$.

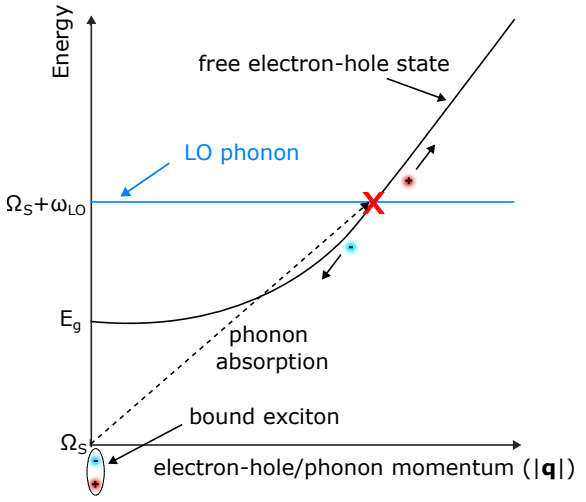

Fig. 1. Schematic of an exciton dissociation process into free electron–hole states, described by Eq. **16** when a material with a band gap of E_g and exciton energy Ω_S absorbs a longitudinal optical (LO) phonon of frequency ω_{LO}, and the condition $\Omega_S + \omega_{LO} > E_g$ is satisfied.

The imaginary part of the exciton–phonon self-energy contains information about the lifetime of excitons due to scattering from phonons into other excitons or free electron–hole pairs (31). As motivated in Fig. 1, the phonon kernel describes scattering from an initial exciton state to a final free electron–hole pair, primarily due to phonon absorption. This process can be formally described within many-body perturbation theory and scattering theory by an $\mathcal{S}$-matrix of the following form (46, 61)

$$\mathcal{S} = 2\pi i\delta[\Omega_S + \omega_{\mathbf{q},\nu} - (E_{c\mathbf{k}} - E_{v\mathbf{k}'})] \times \langle (c\mathbf{k}, v\mathbf{k}'), N_B | K^{ph} | S, N_B + 1 \rangle. \quad [14]$$

The rate τ_S^{-1} of this scattering process described by the $\mathcal{S}$-matrix of Eq. **14** is obtained by taking the time derivative of the square magnitude of this expression. Using the fact that $\delta^2[\Omega_S + \omega_{\mathbf{q},\nu} - (E_{c\mathbf{k}} - E_{v\mathbf{k}'})] = \lim_{t\to\infty} \frac{t}{2\pi}\delta[\Omega_S + \omega_{\mathbf{q},\nu} - (E_{c\mathbf{k}} - E_{v\mathbf{k}'})]$, we arrive at

$$\tau_S^{-1} \approx 2\pi \sum_{c\mathbf{k}v\mathbf{k}'} \delta[\Omega_S + \omega_{\mathbf{q},\nu} - (E_{c\mathbf{k}} - E_{v\mathbf{k}'})] \times |\langle (c\mathbf{k}, v\mathbf{k}'), N_B | K^{ph} | S, N_B + 1 \rangle|^2, \quad [15]$$

in atomic units, where the approximately equal symbol is used because of making the Born approximation, as detailed in *SI Appendix*, section S4. Eq. **15** is the same expression as that obtained through the application of Fermi's golden rule for exciton dissociation, from an initial bound exciton ($|S, N_B + 1\rangle$) to a final free electron–hole ($|(c\mathbf{k}, v\mathbf{k}'), N_B\rangle$) state. This is analogous to the elementary treatment of the photoelectric effect in the hydrogen atom (62).

Defining this scattering process through the $\mathcal{S}$-matrix of Eq. **14** generally requires the initial and final states to be orthogonal to each other (63). We can ensure this is the case within the Born approximation using the theory of rearrangement collisions (64–67), as discussed in more detail in *SI Appendix*, section S4 and also to be presented as a part of a separate work (67). Employing

the optical theorem for the $\mathcal{S}$-matrix of Eq. **14**, the quantity $\mathrm{Im}[K_{SS}^{ph}(\Omega_S, T)]$ can be shown to be equivalent to the rate of the exciton dissociation process depicted in Fig. 1, i.e.

$$2|\mathrm{Im}[K_{SS}^{ph}(\Omega_S, T)]| \approx \tau_S^{-1}(T). \quad [16]$$

Thus, our framework enables the ab initio calculation of exciton dissociation timescales for this particular channel where the products are a free electron and a free hole, for cases in which phonons with $\omega_{\mathbf{q},\nu} > E_B$ dominate. In this regime, $\omega_{\mathbf{q},\nu} > E_B$ exciton dissociation via this channel competes with phonon-mediated exciton–exciton scattering, while exciton–exciton scattering dominates when $\omega_{\mathbf{q},\nu} < E_B$. In what follows below, we will discuss GaN, a system with ultrafast exciton dissociation.

Approximations to the Real Part of the Phonon Kernel

Having established our first-principles formalism to compute the phonon kernel associated with phonon screening, we now explore several common approximations to the real part of this quantity, i.e., the perturbative correction ΔE_B to the exciton binding energy due to phonon screening, at $T = 0$ K. The discussion of these approximations to ΔE_B reveals key physical intuition and connects our work to previous studies. Since for this analysis we restrict ourselves to zero temperatures, we only describe the effect of phonon emission on exciton binding energies.

Fröhlich Electron–Phonon Coupling and Hydrogenic Excitons. Several semiconductors of interest for optoelectronics, such as halide perovskites (25), exhibit electron–phonon coupling dominated by long-range interactions with polar ionic vibrations, which can be described within the Fröhlich model by the operator (68)

$$g_{\mathbf{q}}^{F}(\mathbf{r}) = \frac{i}{|\mathbf{q}|}\left[\frac{4\pi}{NV}\frac{\omega_{LO}}{2}\left(\frac{1}{\epsilon_\infty} - \frac{1}{\epsilon_0}\right)\right]^{\frac{1}{2}} e^{i\mathbf{q}\cdot\mathbf{r}}, \quad [17]$$

where N is the number of unit cells and V the unit cell volume.

Additionally, excitons of a wide class of materials behave in a hydrogenic manner according to the Wannier–Mott limit (69, 70), with the reciprocal space wavefunction of their first excited state ($1s$) expressed as

$$A_{\mathbf{k}} = \frac{(2a_o)^{3/2}}{\pi} \cdot \frac{1}{(1 + a_o^2 k^2)^2}, \quad [18]$$

where $a_o = 1/(2E_B\mu)^{1/2}$ the exciton Bohr radius (in atomic units), $\mathbf{k}$ the wavevector, and μ the exciton effective mass $1/\mu = 1/m_e + 1/m_h$, with m_e and m_h the effective mass of the electron and hole, respectively. Defining the exciton binding energy as $E_B = E_g - \Omega_S$, where E_g is the direct fundamental gap, assuming dispersive parabolic bands for the conduction and valence states, and ignoring the dispersion of the LO phonon, we arrive at the expression (25):

$$\Delta E_B = -\frac{8a_o^3}{\pi^2}\sum_{\mathbf{kq}} \frac{|g_{\mathbf{q}\nu}|^2}{[1 + a_o^2k^2]^2[1 + a_o^2|\mathbf{k}+\mathbf{q}|^2]^2} \times \left[\frac{1}{E_B + \frac{k^2}{2m_e} + \frac{|\mathbf{k}+\mathbf{q}|^2}{2m_h} + \omega_{LO}} + \frac{1}{E_B + \frac{|\mathbf{k}+\mathbf{q}|^2}{2m_e} + \frac{k^2}{2m_h} + \omega_{LO}}\right]. \quad [19]$$

In what follows, we compute this expression numerically for several systems on a grid of $\mathbf{k}$-/$\mathbf{q}$-points and we term the corresponding correction as $\Delta E_B^{\text{F-H}}$ (due to using the Fröhlich and hydrogenic approximations), in order to differentiate it from the full ab initio calculation.

A way to further simplify Eq. **19**, and derive analytic expressions for ΔE_B, is to take the limits $\mathbf{k}/\mathbf{q} \to \mathbf{0}$. We now proceed to explore these limits.

The $\mathbf{k} \to \mathbf{0}$ Limit and the Haken Potential. Following Strinati (11), for excitons that are highly localized around $\mathbf{k} = \mathbf{0}$, we can consider the $\mathbf{k} \to \mathbf{0}$ limit of Eq. **19** and obtain

$$\Delta E_B = \langle 1s|V_{GH}(r)|1s\rangle, \quad [20]$$

where $|1s\rangle$ is the hydrogenic wavefunction and the potential V_{GH} is given by

$$V_{GH}(r) = v(r)\frac{\omega_{LO}}{2\epsilon_*(\omega_{LO} + E_B)}(e^{-r/\tilde{r}_e} + e^{-r/\tilde{r}_h}), \quad [21]$$

with $v(r)$ the bare Coulomb potential and $\frac{1}{\epsilon_*} = (\frac{1}{\epsilon_\infty} - \frac{1}{\epsilon_0})$. The subscript of the potential term V_{GH} indicates this is a generalized Haken potential, having the same form of the so-called Haken potential (23, 24), with the exception that V_{GH} retains the exciton binding energy, which is considered negligible in the derivation presented in ref. 11. We have defined the modified polaron radii for the electron and hole, compared to the usual definition (20), as $\tilde{r}_{e,h} = \frac{1}{\sqrt{2m_{e,h}(\omega_{LO}+E_B)}}$, retaining the exciton binding energy. Therefore, the Haken potential is trivially recovered as an approximation of our ab initio phonon screening expression, via a simplification of Eq. **19**.

With the additional approximation $m_e = m_h$, the expectation value for the shift of the exciton energy due to phonon screening can be expressed in this limit as

$$\Delta E_B^{\mathbf{k}\to\mathbf{0}} = -\frac{2\omega_{LO}\left(1 - \frac{\epsilon_\infty}{\epsilon_0}\right)}{\left(1 + \frac{\omega_{LO}}{E_B}\right)\left(1 + \frac{1}{\sqrt{2}}\sqrt{1 + \frac{\omega_{LO}}{E_B}}\right)^2}. \quad [22]$$

The $\mathbf{q} \to \mathbf{0}$ Limit. While the Haken potential is based on taking $\mathbf{k} \to 0$ with the justification of a highly localized exciton in reciprocal space, ref. 25 instead retained the $\mathbf{k}$ dependence and considered the limit $\mathbf{q} \to 0$ for the potential term in the expectation value of Eq. **19** for the shift of the exciton binding energy. This is more justified in materials with highly dispersive electronic bands, where setting the electronic momentum to zero can constitute an oversimplification. For such systems, the momentum $\mathbf{q}$ of a phonon may be considered

negligible compared to that of an electron or a hole. Using this approximation we obtain

$$\Delta E_B = \langle 1s|V^{\mathbf{q}\to\mathbf{0}}(r)|1s\rangle, \quad [23]$$

where

$$V^{\mathbf{q}\to\mathbf{0}}(r) = v(r)\frac{a_o^2\omega_{LO}}{\epsilon_*(\omega_{LO}+E_B)} \cdot\left[\frac{1}{a_o^2-b_o^2}-\frac{1}{r}\cdot\frac{2a_ob_o^2}{(a_o^2-b_o^2)^2}\left(1-e^{-(\frac{1}{b_o}-\frac{1}{a_o})r}\right)\right], \quad [24]$$

with a_o the exciton Bohr radius and $b_o = \sqrt{\frac{1}{2\mu(\omega_{LO}+E_B)}}$. By setting $m_e = m_h$, the expectation value of Eq. **23** is found to be

$$\Delta E_B^{\mathbf{q}\to\mathbf{0}} = -2\omega_{LO}\left(1-\frac{\epsilon_\infty}{\epsilon_0}\right)\frac{\sqrt{1+\frac{\omega_{LO}}{E_B}}+3}{\left(1+\sqrt{1+\frac{\omega_{LO}}{E_B}}\right)^3}, \quad [25]$$

the result derived in ref. 25. We will see when discussing our computational results that this limit yields results which are generally significantly closer to the full ab initio value for the shift of the exciton energy compared to the generalized Haken ($\mathbf{k}\to\mathbf{0}$) case.

Ab Initio Results for Select Systems

Comparison between Ab Initio and Limiting Cases at 0 K. We start with the ab initio phonon screening correction to the exciton binding energy at 0 K, and the values predicted through the various approximations outlined previously. The results for the different systems studied in this work are summarized in Table 1. Details on the structure of the studied materials as well as computational details are given in *SI Appendix*, section S1, with the convergence properties of the phonon kernel discussed in more detail in *SI Appendix*, section S5. We note that while here we focus on spin-singlet excitons, our formalism could also be applied to triplets.

Firstly, we note that for all studied systems, the ab initio value for the shift of the exciton binding energy due to phonon screening (as given by Eq. **11**) falls between the values of the two limiting cases $\Delta E_B^{k\to 0}$ and $\Delta E_B^{q\to 0}$. The former of these limits, which corresponds to the well-known Haken potential, consistently underestimates $\Delta E_B^{\text{ab initio}}$, while the $q\to 0$ limit leads to a small overestimation. As introduced by Haken (23, 24) and also elaborated by Strinati (11), exciton coefficients in several semiconductors, are highly localized around $\mathbf{k}=\mathbf{0}$ in reciprocal space, motivating the $k\to 0$ approximation. However, this approximation also suggests that one may neglect the dispersion of electronic bands, only retaining the finite dispersion of the LO phonon. In materials such as the ones studied here, $A_{\mathbf{k}}$ assume appreciable nonzero values away from Γ, and this approximation is no longer valid, leading to the observed poor agreement between $\Delta E_B^{k\to 0}$ and $\Delta E_B^{\text{ab initio}}$. For the systems investigated in this work, considering the momentum of phonons to be negligible compared to that of the electrons, i.e., taking the $q\to 0$ in the energy denominators of Eq. **19** and leading to the expression of Eq. **25**, is physically better justified, leading to better agreement with first-principles calculations.

Moreover, the correction $\Delta E_B^{\text{F-H}}$, obtained through numerical integration of Eq. **19**, which only assumes hydrogenic excitons and an electron–phonon interaction governed by the Fröhlich vertex, is in excellent agreement with the first-principles results, for all systems but $SrTiO_3$, for reasons discussed in detail below. For the remaining systems studied here, the hydrogenic and Fröhlich approximation are well justified, as discussed in ref. 25, leading to the excellent agreement between $\Delta E_B^{\text{F-H}}$ and $\Delta E_B^{\text{ab initio}}$. The effective masses entering Eq. **19** are given in *SI Appendix*, section S2. Two of the studied materials, AlN and GaN are in their wurtzite phase and hence anisotropic, we therefore use effective masses averaged across the three crystallographic axes.

First-Principles Calculations of Finite Temperature Exciton Binding Energies and Dissociation Timescales. In what follows, we will employ the fully first-principles phonon kernel and focus on temperature-dependent effects of phonon screening on excitons, in three of the materials selected from Table 1. Specifically, we focus on CdS, the material with the lowest LO phonon frequency, which indicates the potential of this material for exhibiting substantial temperature-dependent phonon screening. Additionally, GaN is the only system studied here with $\omega_{LO} > E_B$; thus, the absorption of an LO phonon from the exciton may lead to dissociation of the electron–hole pair, according to Eq. **16**. Finally, we discuss the effects of phonon screening on the cubic perovskite phase of $SrTiO_3$, which has a very large ϵ_0 value, and is the only material in this work showing significant deviations between the ab initio and $\Delta E_B^{\text{F-H}}$ corrections to the exciton binding energy at 0 K. In *SI Appendix*, section S6, we estimate the effects of thermal expansion on the phonon screening of excitons, which we generally find to be small. As also discussed in *SI Appendix*, section S6, thermal expansion can cause a modest reduction of the exciton binding energy, additional to that caused by phonon screening, leading to overall improved agreement with experiment. Nevertheless,

Table 1. Comparison of the shift of the exciton binding energy at 0 K due to phonon screening in the different studied systems

System	E_B	ω_{LO}	ϵ_∞	ϵ_0	$\Delta E_B^{\text{ab initio}}$	$\Delta E_B^{k\to 0}$ (Eq. **22**)	$\Delta E_B^{q\to 0}$ (Eq. **25**)	$\Delta E_B^{\text{F-H}}$ (Eq. **19**)
GaN	65	87	5.9	10.8	−15	−6	−22	−15
AlN	143	110	4.5	8.7	−29	−16	−36	−29
MgO	327	84	3.3	11.3	−46	−26	−52	−48
CdS	39	34	6.2	10.4	−6	−3	−9	−6
$SrTiO_3$	122	98	6.2	409	−44	−25	−65	−51

All energy values are given in meV. For reference, the computed value of the exciton binding energy E_B as obtained from the solution of the bare BSE (without phonon effects) is given here, alongside the values computed within DFPT for the LO phonon frequency and the high-/low-frequency dielectric constants $\epsilon_{\infty,o}$.

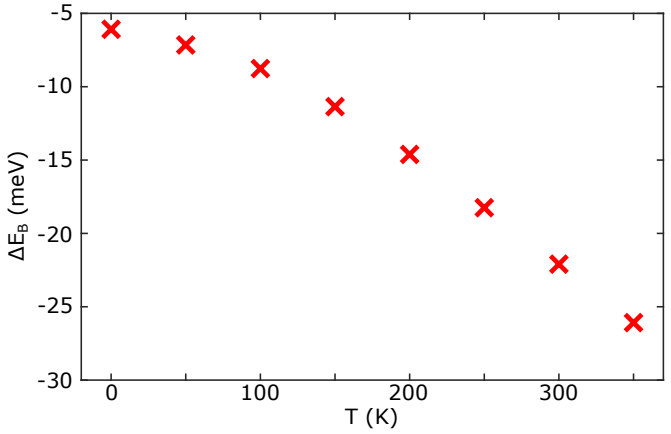

Fig. 2. Calculated shift of the exciton binding energy of CdS due to phonon screening, as a function of temperature.

phonon screening remains the dominant effect that determines the temperature dependence of exciton binding energies.

CdS. In Fig. 2, we find that the correction of the exciton binding energy of CdS due to phonon screening is strongly temperature-dependent. The low-temperature correction is equal to almost −6 meV, and becomes more significant at room temperature, where it reaches a value of −22 meV. This suggests that the bare, clamped-ion exciton binding energy of CdS of 39 meV as computed from BSE (Table 1), will be renormalized by more than 50%, to 17 meV at 300 K, due to phonon screening. The experimental value for the exciton binding energy has been reported at low temperatures to be 28 to 30 meV (71–73), in good agreement with our low-temperature result of a corrected exciton binding energy of 33 meV. Experimental temperature-dependent studies of CdS excitons assume the exciton binding energy to be temperature-independent (73), and extract it as the activation energy of a fit of photoluminescence data. Our results show that through the phonon modification of the BSE kernel, the excitonic interactions become themselves temperature-dependent, resulting in the strong temperature dependence of the exciton binding energy of CdS shown in Fig. 2.

It is instructive to decompose the computed phonon-induced screening correction to the exciton binding energy into contributions from different phonon branches of CdS. As seen in Fig. 3, unsurprisingly the vast majority of this effect is driven by the LO phonon with an average frequency of 34 meV across the Brillouin zone. The contribution of this phonon to ΔE_B increases substantially with temperature, due to its low frequency and high thermal activation. Interestingly, we also find that at finite temperatures there is a nonnegligible contribution of acoustic phonons to the screening, which is strongly temperature-dependent due to the large thermal occupation factors of these modes. This contribution of acoustic modes to the phonon screening of excitons is generally present in piezoelectric materials such as CdS, as we discuss in more detail in *SI Appendix*, section S7. Moreover, Eq. **9** allows us to identify the separate contributions of phonon absorption and emission to the phonon kernel. As shown in *SI Appendix*, section S8, phonon emission is already active at low temperatures, while phonon absorption only provides a minor contribution. As the temperature increases, the contribution of phonon absorption to the screening of the exciton becomes more substantial, and eventually emission and absorption contribute equally. Moreover, in *SI Appendix*, section S8, and specifically *SI Appendix*, Figs. S6–S9, we show the dependence of the mode-resolved contributions to ΔE_B on the phonon wavevector $|\mathbf{q}|$, and the dominant contribution of the LO phonons follows a Fröhlich-like $1/|\mathbf{q}|^2$ dependence.

GaN. The value of ΔE_B for GaN only shows weak temperature dependence as seen in Fig. 4, since the frequency of its LO phonon has a value of 84 meV, significantly above room temperature. As for CdS, ΔE_B is dominated by the LO phonon (Fig. 5), while here too, there is a small but nonnegligible contribution from acoustic phonons, due to GaN being a piezoelectric material; see *SI Appendix*, section S7.

Solution of the bare BSE gives an exciton binding energy of $E_B = 65$ meV for GaN, and by including the correction due to phonon screening we predict it will decrease to 46 meV at 300 K. The experimental values for the exciton binding energy of GaN are within the range of 20 to 28 meV (74, 75), with some studies measuring this quantity at room temperature (75) and others at cryogenic temperatures (74). We were not able to find a systematic experimental study on the temperature dependence of the exciton binding energy; however, it is clear that while inclusion of phonon screening effects leads to better agreement with experiment, we still overestimate the exciton binding energy, similar to the case of the halide perovskites (25). This result could be attributed to the fact that the magnitude of electron–phonon interaction within DFPT might be underestimated compared to using higher-level theories (48, 76, 77), as well as to the fact that

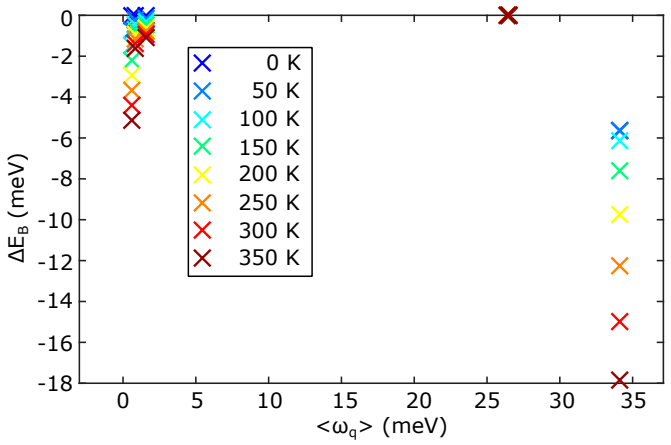

Fig. 3. Contribution of different phonon modes to the exciton binding energy shift of CdS due to phonon screening, as a function of temperature. Here, $\langle\omega_q\rangle$ denotes the average frequency of a particular phonon branch.

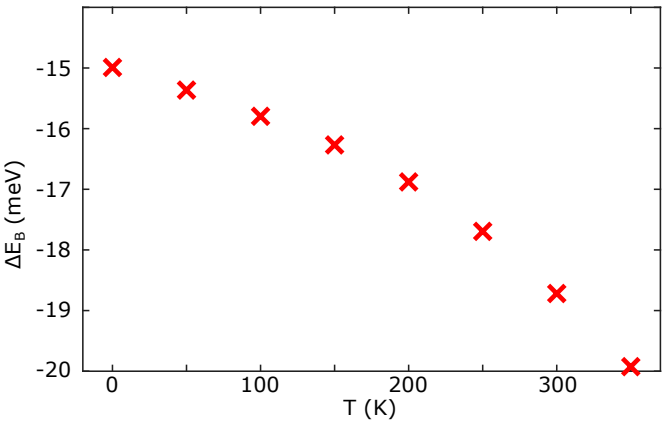

Fig. 4. Calculated shift of the exciton binding energy of GaN due to phonon screening, as a function of temperature.

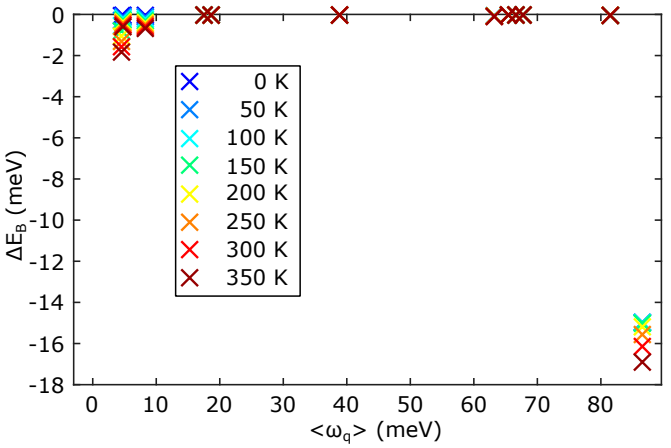

Fig. 5. Contribution of different phonon modes to the exciton binding energy shift of GaN due to phonon screening, as a function of temperature. Here, $\langle\omega_q\rangle$ denotes the average frequency of a particular phonon branch across the studied patch of the Brillouin zone.

we do not account for polaronic interference effects as discussed previously.

Among the systems studied in this work, GaN is the only one for which $\omega_{LO} > E_B$, making it a case where the absorption of a single LO phonon by the exciton might lead to its dissociation into a free electron–hole pair. The fact that $\omega_{LO} > E_B$ manifests as a finite value of $\mathrm{Im}[K_{SS}^{ph}(\Omega_S, T)]$, as shown in Fig. 6*A*. The value of η in Eq. **9** represents a small arbitrary broadening we introduce to the energy levels appearing in the denominator, in order to resolve the crossing between an exciton that has absorbed a phonon, and the free electron–hole pair, as schematically shown in Fig. 1. Given the fine grid we are employing here ($100 \times 100 \times 100$), we find that values of η within the range of 0.5 to 2 meV are sufficient to satisfy this energy conservation condition. In Fig. 6*A*, we plot $\mathrm{Im}[K_{SS}^{ph}(\Omega_S, T)]$ for a range of η values within that window and find that the change in the result is minor. Our values for $\mathrm{Im}[K_{SS}^{ph}(\Omega_S, T)]$ are similar to the imaginary part of the self-energy of a model system (31), representing phonon-mediated exciton–exciton scattering, indicating that these effects are directly competing.

In Fig. 6*B* we plot the exciton dissociation timescale for the lowest singlet exciton of GaN using Eq. **16**, as a function of temperature and for different values of η. This exciton dissociation process is entirely due to the absorption of LO phonons by the exciton, as no other phonons contribute to the imaginary part of the phonon kernel (Fig. 7). We see from Fig. 6*B* that at low temperatures, the exciton dissociation timescale varies significantly with changes in the value of η. This is due to the fact that the imaginary part of the phonon kernel for temperatures up to approximately 150 K assumes very small values of less than 0.5 meV, making even small changes in η significant for its inverse in Eq. **16**. Nevertheless, the exciton dissociation timescale τ becomes more stable with respect to changes in the value of η at higher temperatures, as also highlighted in the inset of Fig. 6*B*. At 300 K we find $\tau = 111$ fs. While we have not found experimental studies on time-resolved exciton dissociation in GaN to compare against, it is encouraging that recent experiments employing ultrafast 2D electronic spectroscopy report exciton dissociation timescales that are similar to what we compute here, for semiconductors with comparable exciton binding energies. Specifically, for GaSe an exciton dissociation timescale of 112 fs at room temperature has been reported (78), while for $CH_3NH_3PbI_3$, an exciton dissociation timescale of approximately 50 fs (79) was found.

It is also worth pointing out that the finite exciton lifetime described by the imaginary part of the phonon kernel, will manifest as a finite linewidth in absorption and emission spectra. However, exciton dissociation will only be one of several scattering processes contributing to the overall linewidth observed in experiment, with phonon-mediated exciton–exciton scattering (40), Auger recombination (80), and more, all contributing to the total linewidth. It is therefore no surprise that our value of approximately 3 meV for the imaginary part of the phonon kernel of GaN at 300 K is substantially smaller than the experimental linewidth of approximately 20 meV at the same temperature (81).

$SrTiO_3$. Among the systems of Table 1, $SrTiO_3$ is the only one for which we find a substantial difference in the value of $\Delta E_B^{\text{F-H}}$ at 0 K as predicted from the numerical integration of Eq. **19**, and the full ab initio correction $\Delta E_B^{\text{ab initio}}$ to the exciton binding energy, following Eq. **9**. Moreover, this is a system with a very large value for the low-frequency dielectric constant ϵ_0, indicating a potentially very large contribution of phonons to the screened Coulomb interaction, making it particularly interesting for further study.

In Fig. 8, we visualize the temperature-dependent correction ΔE_B to the exciton binding energy for this system, which we

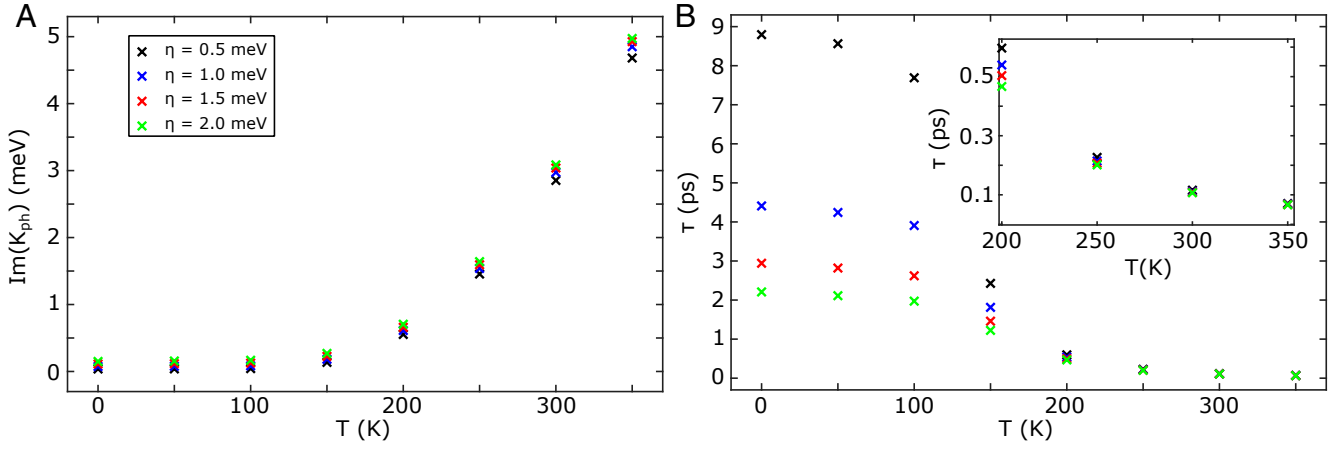

Fig. 6. Imaginary part of the phonon kernel matrix elements between the 1*s* exciton basis states (*A*) and associated calculated timescale for exciton dissociation (*B*) as a function of temperature and the η parameter for GaN. The *Inset* of panel *B* provides a closer view of the range of temperatures around 300 K.

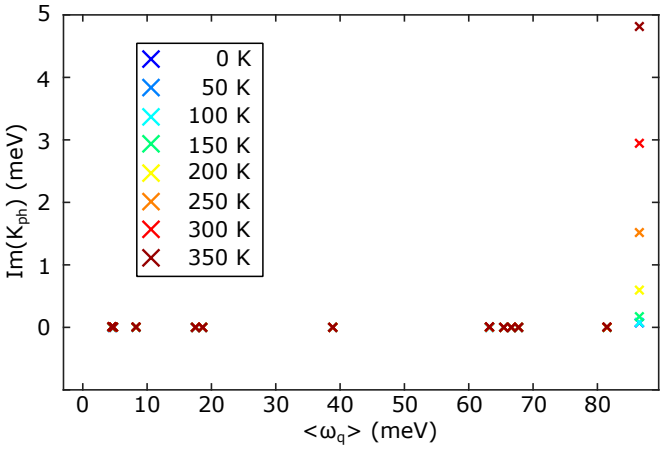

Fig. 7. Contribution of different phonon modes to the imaginary part of the phonon kernel of GaN, as a function of temperature and for $\eta = 1$ meV. Here, $\langle \omega_q \rangle$ denotes the average frequency of a particular phonon branch across the studied patch of the Brillouin zone.

find to be equal to −52 meV at 300 K, renormalizing the bare clamped-ion exciton binding energy as computed within BSE by 43%, from 122 meV to 70 meV. By decomposing this correction to the effect of individual phonons in Fig. 9, we find that while phonon screening in this system is dominated by the LO mode with a frequency of 98 meV (henceforth referred to as LO-1), there is a substantial contribution from an LO phonon with a lower frequency of 57 meV (henceforth referred to as LO-2), which has been discussed previously to also exhibit Fröhlich-like coupling (82).

The reason behind the disagreement of the ab initio and $\Delta E_B^{\text{F-H}}$ results for the correction to the exciton binding energy is that $SrTiO_3$ has multiple phonon modes contributing to the phonon screening and the static dielectric constant ϵ_0. In these cases, the Fröhlich model, which is used in the numerical integration of Eq. **19**, breaks down, and one needs to instead use the generalized Fröhlich vertex of ref. 83. For a phonon ν, this is written as

$$g_{\mathbf{q},\nu} = i\frac{4\pi}{V}\sum_j \left(\frac{1}{2NM_j\omega_{\mathbf{q},\nu}}\right)^{1/2} \cdot \frac{\mathbf{q}\cdot\mathbf{Z}_j\cdot e_{\mathbf{j},\nu}(\mathbf{q})}{\mathbf{q}\cdot\epsilon_\infty\cdot\mathbf{q}}, \qquad [26]$$

in atomic units. For atom j, $\mathbf{Z}_j$ is its Born effective charge tensor and M_j its mass, while V the unit cell volume, N the number of unit cells, and $e_{\mathbf{j},\nu}(\mathbf{q})$ the phonon eigenvectors. In Table 2,

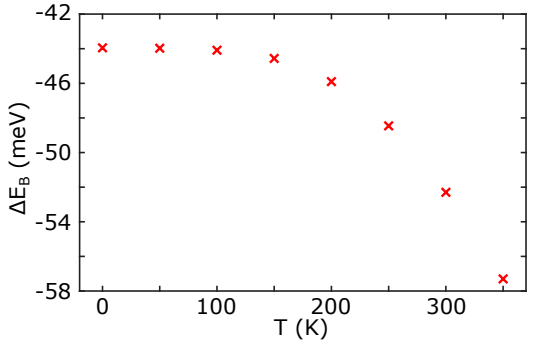

Fig. 8. Calculated shift of the exciton binding energy of $SrTiO_3$ due to phonon screening, as a function of temperature.

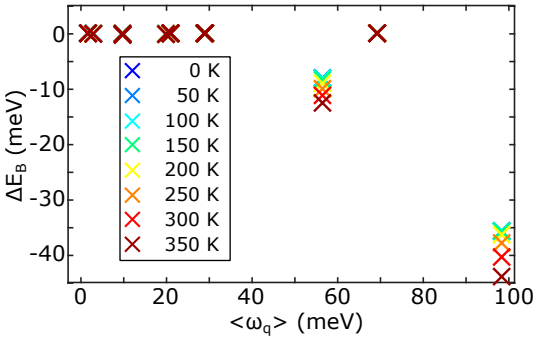

Fig. 9. Contribution of different phonon modes to the exciton binding energy shift of $SrTiO_3$ due to phonon screening, as a function of temperature. Here, $\langle \omega_q \rangle$ denotes the average frequency of a particular phonon branch across the studied patch of the Brillouin zone.

we show that employing this generalized Fröhlich vertex in the numerical integration of Eq. **19** gives excellent agreement with the ab initio result for the correction to the exciton binding energy of $SrTiO_3$ due to its LO-1 and LO-2 phonons. On the other hand, numerically integrating Eq. **19** for the LO-1 and LO-2 phonons using the standard Fröhlich vertex of Eq. **17** leads to significant discrepancies with the ab initio results. The comparison between the case where we use the Fröhlich and hydrogenic approximations, and the ab initio result, is discussed in more detail in *SI Appendix*, section S9.

Discussion, Conclusions, and Outlook

In this work, we have developed an ab initio framework for computing the temperature-dependent phonon kernel of semiconductors and insulators associated with phonon screening, according to Eq. **9**. We show how approximations to the phonon kernel lead to the model expressions of Eqs. **19**, **22**, and **25**, some of which have been widely discussed in the literature. Compared to utilizing these model expressions, our ab initio approach does not rely on any restrictive approximations, treating the effect of all phonon modes on equal footing in phonon screening, without any assumption about the nature of their coupling to electrons. It also allows us to extend our results to finite temperatures in a straightforward manner, and to go beyond the Wannier–Mott model, which will be critical in systems where excitons are not hydrogenic in nature (60). Additionally, the imaginary part of the phonon kernel in the exciton basis allows us to extract information about temperature-dependent exciton dissociation processes to free electrons and holes in certain limits. Overall, having access to the full, temperature-dependent complex phonon kernel enhances our ability to predict excitonic properties including phonon screening, while providing physical

Table 2. Phonon-resolved screening of the exciton binding energy of $SrTiO_3$ by the two LO modes of this material at 0 K (in meV)

Phonon mode	$\Delta E_B^{\text{F-H}}$	$\Delta E_{B,\text{gen.}}^{\text{F-H}}$	$\Delta E_B^{\text{ab initio}}$
LO-1	−51	−38	−36
LO-2	−34	−8	−8

We compare full ab initio level theory ($\Delta E_B^{\text{ab initio}}$), the numerical integration of Eq. **19** using the standard Fröhlich vertex for each phonon ($\Delta E_B^{\text{F-H}}$), as well as the numerical integration of Eq. **19** employing the generalized Fröhlich vertex ($\Delta E_{B,\text{gen.}}^{\text{F-H}}$).

insights, with some of the ones obtained in this work summarized below.

Firstly, we found that for bulk CdS, phonon screening reduces the bare BSE exciton binding energy by more than 50% at room temperature, demonstrating that the effect of phonon screening on excitons can be very strong and highly temperature-dependent. Our theoretical framework provides a temperature-dependent correction to the BSE kernel and therefore to the excitonic interactions. Indeed, experimental studies in the 1970s and 1980s found indications of strongly temperature-dependent excitonic interactions, but were unable to quantify this effect (84–86). These modified interactions can lead to strongly temperature-dependent exciton binding energies, as recent experimental studies have found (87, 88), and at odds with the common assumption of a temperature-independent exciton binding energy (73, 81).

Our formalism describes the screening of the exciton due to both processes of emission and absorption of phonons, which contribute equally to the reduction of the exciton binding energy at 300 K, while phonon emission processes entirely dominate at low temperatures. Additionally, we found an important reduction of the exciton binding energy due to screening from acoustic phonons, which is present in piezoelectric materials. This important reduction of the exciton binding energy due to phonon screening, a nonadiabatic effect, demonstrates that approaches based on trajectory-based adiabatic methods may underestimate the effect of ionic screening on exciton binding energies (13), similar to how the adiabatic approximation can lead to significant errors in computed band gap renormalizations (89).

Importantly, having access to the imaginary part of the phonon kernel allows us to compute exciton dissociation rates via single-phonon emission and absorption processes entirely from first principles. For the case of GaN where $E_B < \omega_{LO}$, the absorption of a LO phonon is sufficient to dissociate the exciton and generate a free electron–hole pair. Our computed exciton dissociation timescale for this system is approximately 111 fs at 300 K. While we have not found experimental exciton dissociation timescales for GaN to compare against, it is encouraging that our predicted value is reasonably close to experimental values obtained in semiconductors with comparable exciton binding energies, such as GaSe with an exciton dissociation timescale of 112 fs (78), and $CH_3NH_3PbI_3$ with an exciton dissociation timescale of approximately 50 fs (79).

Moving forward, our first-principles approach could be extended in multiple ways. For example, one could re-solve the BSE nonperturbatively upon correction of the electronic BSE kernel, which might substantially change the exciton wavefunction and computed absorption spectra for systems where the phonon kernel in the bare exciton basis has large off-diagonal entries. Here, we have used the harmonic approximation within DFPT, which is justified for the studied systems, given that phonon screening is dominated by higher frequency LO phonons, which are generally harmonic. However, one could incorporate anharmonic effects into phonon screening calculations, which can be important for screening from low-frequency phonons (82). Furthermore, one could consider the interplay of phonon screening with the effects of polaronic mass enhancement and polaron interference on excitons (19, 20) by incorporating the Fan-Migdal term and higher-order diagrams into this approach. Our approach for ensuring gauge consistency between interpolated electron–phonon matrix elements and exciton coefficients could be extended to account for the effects of phonon screening and other diagrams on finite-momentum excitons (31), by utilizing recent schemes for exciton Wannier functions (90). While in this work we have studied some representative semiconducting materials, we hope our first-principles approach will be widely adopted and used to study the effect of phonons on dissociating and screening excitons in diverse materials of interest for a variety of technological applications, such as heterostructures of two-dimensional semiconductors, quantum wells, or doped systems.

Materials and Methods

Computational details for all DFT and *GW*-BSE calculations on the studied systems, as well as details on the convergence of phonon screening with respect to the k-point grid and the number of exciton states accounted for in the phonon kernel, are provided in *SI Appendix*. Moreover, *SI Appendix* includes the estimated exciton and polaron radii of the systems studied here, as well as extended derivations of the finite-temperature expression Eq. **9** within the Matsubara formalism, and of the exciton dissociation scattering rate described by the imaginary part of K^{ph}. An extended discussion is also provided on the effect of thermal expansion on the exciton binding energies and on phonon screening, on the role of acoustic modes in screening the excitons of piezoelectric materials, the wavevector dependence of phonon screening, the relative contribution of phonon emission and phonon absorption to screening of excitons, as well as an extended discussion of phonon screening in $SrTiO_3$, and the reasons underlying the failure of the different model approaches in this system to reproduce the full first-principles result.

Data, Materials, and Software Availability. All study data are included in the article and/or *SI Appendix*.

ACKNOWLEDGMENTS. We acknowledge useful discussions with Stephen E. Gant (University of California at Berkeley). This work was primarily supported by the Theory of Materials program, which provided *GW* and *GW*-BSE calculations and analysis of phonon effects, and the Center for Computational Study of Excited-State Phenomena in Energy Materials as part of the Computational Materials Sciences Program, which provided advanced codes, at the Lawrence Berkeley National Laboratory, funded by the U.S. Department of Energy, Office of Science, Basic Energy Sciences, Materials Sciences and Engineering Division, under Contract No. DE-AC02-05CH11231. Z.L. and S.G.L. acknowledge support from the NSF under Grant No. OAC-2103991 in the development of interoperable software enabling the EPW and BerkeleyGW calculations with consistent gauge. Computational resources were provided by the National Energy Research Scientific Computing Center. C.J.N.C. and M.R.F. acknowledge support from the UK Engineering and Physical Sciences Research Council (EPSRC).

Author affiliations: [a]KBR, Inc., NASA Ames Research Center, Moffett Field, CA 94035; [b]Materials Sciences Division, Lawrence Berkeley National Laboratory, Berkeley, CA 94720; [c]Department of Materials Science and Engineering, Stanford University, Stanford, CA 94305; [d]Mork Family Department of Chemical Engineering and Materials Science, University of Southern California, Los Angeles, CA 90089; [e]Department of Physics, University of California Berkeley, Berkeley, CA 94720; [f]Department of Physics, University of Oxford, Oxford OX1 3PJ, United Kingdom; and [g]Kavli Energy NanoScience Institute at Berkeley, Berkeley, CA 94720

1. G. Grancini *et al.*, Hot exciton dissociation in polymer solar cells. *Nat. Mater.* **12**, 29–33 (2013).
2. T. J. Savenije *et al.*, Thermally activated exciton dissociation and recombination control the carrier dynamics in organometal halide perovskite. *J. Phys. Chem. Lett.* **5**, 2189–2194 (2014).
3. X. Ai *et al.*, Efficient radical-based light-emitting diodes with doublet emission. *Nature* **563**, 536–540 (2018).
4. S. Reineke *et al.*, White organic light-emitting diodes with fluorescent tube efficiency. *Nature* **459**, 234–238 (2009).
5. L. Hedin, New method for calculating the one-particle Green's function with application to the electron-gas problem. *Phys. Rev.* **139**, 796–823 (1965).
6. M. S. Hybertsen, S. G. Louie, Electron correlation in semiconductors and insulators: Band gaps and quasiparticle energies. *Phys. Rev. B* **34**, 5390–5413 (1986).
7. S. Albrecht, L. Reining, R. Del Sole, G. Onida, Ab initio calculation of excitonic effects in the optical spectra of semiconductors. *Phys. Rev. Lett.* **80**, 4510–4513 (1998).

8. L. X. Benedict, E. L. Shirley, R. B. Bohn, Optical absorption of insulators and the electron–hole interaction: An ab initio calculation. *Phys. Rev. Lett.* **80**, 4514–4517 (1998).
9. M. Rohlfing, S. G. Louie, Electron–hole excitations in semiconductors and insulators. *Phys. Rev. Lett.* **81**, 2312–2315 (1998).
10. M. Rohlfing, S. G. Louie, Electron–hole excitations and optical spectra from first principles. *Phys. Rev. B, Condens. Matter Mater. Phys.* **62**, 4927–4944 (2000).
11. G. Strinati, Application of the Green's functions method to the study of the optical properties of semiconductors. *La Rivist. Del Nuovo Cim. Ser.* **3**, 1–86 (1988).
12. D. M. Ceperley, B. J. Alder, Ground state of the electron gas by a stochastic method. *Phys. Rev. Lett.* **45**, 566–569 (1980).
13. M. Bokdam *et al*., Role of polar phonons in the photo excited state of metal halide perovskites. *Sci. Rep.* **6**, 1–8 (2016).
14. F. Bechstedt, J. Furthmüller, Influence of screening dynamics on excitons in Ga_2O_3 polymorphs. *Appl. Phys. Lett.* **114**, 6–10 (2019).
15. P. Umari, E. Mosconi, F. De Angelis, Infrared dielectric screening determines the low exciton binding energy of metal-halide perovskites. *J. Phys. Chem. Lett.* **9**, 620–627 (2018).
16. A. Schleife *et al*., Optical properties of In_2O_3 from experiment and first-principles theory: Influence of lattice screening. *New J. Phys.* **20**, 053016 (2018).
17. F. Fuchs, C. Rödl, A. Schleife, F. Bechstedt, Efficient $O(N_2)$ approach to solve the Bethe–Salpeter equation for excitonic bound states. *Phys. Rev. B, Condens. Matter Mater. Phys.* **78**, 1–13 (2008).
18. Y. Park, D. T. Limmer, Renormalization of excitonic properties by polar phonons. *J. Chem. Phys.* **157**, 104116 (2022).
19. S. D. Mahanti, C. M. Varma, Effective electron and hole interactions in a polarizable field. *Phys. Rev. Lett.* **25**, 1115 (1970).
20. S. D. Mahanti, C. M. Varma, Effective electron–hole interactions in polar semiconductors. *Phys. Rev. B* **6**, 2209 (1972).
21. L. M. Herz, How lattice dynamics moderate the electronic properties of metal-halide perovskites. *J. Phys. Chem. Lett.* **9**, 6853–6863 (2018).
22. L. Adamska, P. Umari, Bethe–Salpeter equation approach with electron–phonon coupling for exciton binding energies. *Phys. Rev. B* **103**, 75201 (2021).
23. H. Haken, Zur quantentheorie des mehrelektronensystems im schwingenden gitter I. *Z. Phys.* **146**, 527–554 (1956).
24. H. Haken, Die theorie des exzitons im festen korper. *Fort. Phys.* **6**, 271–334 (1958).
25. M. R. Filip, J. B. Haber, J. B. Neaton, Phonon screening of excitons in semiconductors: Halide perovskites and beyond. *Phys. Rev. Lett.* **127**, 67401 (2021).
26. G. Baym, Field-theoretic approach to the properties of the solid state. *Ann. Phys.* **14**, 1–42 (1961).
27. L. Hedin, New method for calculating the one-particle Green's function with application to the electron-gas problem. *Phys. Rev.* **139**, 796 (1965).
28. F. Giustino, Electron–phonon interactions from first principles. *Rev. Mod. Phys.* **89**, 1–63 (2017).
29. L. Hedin, S. Lundqvist, Effects of electron–electron and electron–phonon interactions on the one-electron states of solids. *Solid State Phys.: Adv. Res. Appl.* **23**, 1–181 (1970).
30. P. Cudazzo, First-principles description of the exciton–phonon interaction: A cumulant approach. *Phys. Rev. B* **102**, 1–11 (2020).
31. G. Antonius, S. G. Louie, Theory of exciton–phonon coupling. *Phys. Rev. B* **105**, 85111 (2022).
32. F. Paleari, A. Marini, Exciton–phonon interaction calls for a revision of the "exciton" concept. *Phys. Rev. B* **106**, 1–16 (2022).
33. Y. Toyozawa, Theory of line-shapes of the exciton absorption bands. *Progr. Theor. Phys.* **20**, 53–81 (1958).
34. F. Paleari, H. P. Miranda, A. Molina-Sánchez, L. Wirtz, Exciton–phonon coupling in the ultraviolet absorption and emission spectra of bulk hexagonal boron nitride. *Phys. Rev. Lett.* **122**, 187401 (2019).
35. E. Cannuccia, B. Monserrat, C. Attaccalite, Theory of phonon-assisted luminescence in solids: Application to hexagonal boron nitride. *Phys. Rev. B* **99**, 1–5 (2019).
36. P. Lechifflart, F. Paleari, D. Sangalli, C. Attaccalite, First-principles study of luminescence in hexagonal boron nitride single layer: Exciton–phonon coupling and the role of substrate. *Phys. Rev. Mater.* **7**, 24006 (2023).
37. A. M. Alvertis, J. B. Haber, E. A. Engel, S. Sharifzadeh, J. B. Neaton, Phonon-induced localization of excitons in molecular crystals from first principles. *Phys. Rev. Lett.* **130**, 86401 (2023).
38. A. M. Alvertis *et al*., Impact of exciton delocalization on exciton–vibration interactions in organic semiconductors. *Phys. Rev. B, Condens. Matter Mater. Phys.* **102**, 081122(R) (2020).
39. H. Y. Chen, D. Sangalli, M. Bernardi, Exciton–phonon interaction and relaxation times from first principles. *Phys. Rev. Lett.* **125**, 107401 (2020).
40. Y. H. Chan *et al*., Exciton lifetime and optical line width profile via exciton–phonon interactions: Theory and first-principles calculations for monolayer MoS_2. *Nano Lett.* **23**, 3971–3977 (2023).
41. G. Cohen, J. B. Haber, J. B. Neaton, D. Y. Qiu, S. Refaely-Abramson, Phonon-Driven Femtosecond Dynamics of Excitons in Crystalline Pentacene from First Principles. *Phys. Rev. Lett.* **132**, 126902 (2024).
42. J. Pollmann, H. Büttner, Effective Hamiltonians and bindings energies of Wannier excitons in polar semiconductors. *Phys. Rev. B* **16**, 4480–4490 (1977).
43. C. D. Spataru, F. Léonard, Tunable band gaps and excitons in doped semiconducting carbon nanotubes made possible by acoustic plasmons. *Phys. Rev. Lett.* **104**, 1–4 (2010).
44. X. Zhang, J. A. Leveillee, A. Schleife, Effect of dynamical screening in the Bethe-Salpeter framework: Excitons in crystalline naphthalene. *Phys. Rev. B* **107**, 235205 (2023).
45. A. Champagne *et al*., Quasiparticle and optical properties of carrier-doped monolayer $MoTe_2$ from first principles. *Nano Lett.* **23**, 4274 (2023).
46. G. D. Mahan, *Many-Particle Physics, Physics of Solids and Liquids* (Springer, 2013).
47. S. Baroni, S. De Gironcoli, A. Dal Corso, Phonons and related crystal properties from density-functional perturbation theory. *Rev. Mod. Phys.* **73**, 515 (2001).
48. Z. Li, G. Antonius, M. Wu, F. H. Da Jornada, S. G. Louie, Electron–phonon coupling from ab initio linear-response theory within the GW method: Correlation-enhanced interactions and superconductivity in $Ba_{1-x}K_xBiO_3$. *Phys. Rev. Lett.* **122**, 186402 (2019).
49. N. E. Lee, J. J. Zhou, H. Y. Chen, M. Bernardi, Ab initio electron-two-phonon scattering in GaAs from next-to-leading order perturbation theory. *Nat. Commun.* **11**, 1607 (2020).
50. F. Giustino, M. L. Cohen, S. G. Louie, Electron–phonon interaction using Wannier functions. *Phys. Rev. B, Condens. Matter Mater. Phys.* **76**, 1–19 (2007).
51. X. W. Zhang, K. Xie, E. G. Wang, T. Cao, X. Z. Li, Phonon-mediated exciton relaxation in two-dimensional semiconductors: Selection rules and relaxation pathways. arXiv [Preprint] (2021). https://doi.org/10.48550/arXiv.2110.08873 (Accessed 3 April 2023).
52. X. W. Zhang, T. Cao, Ab initio calculations of spin-nonconserving exciton-phonon scattering in monolayer transition metal dichalcogenides. *J. Phys. Condens. Matter* **34**, 264002 (2022).
53. A. M. Alvertis *et al*., Importance of nonuniform Brillouin zone sampling for ab initio Bethe–Salpeter equation calculations of exciton binding energies in crystalline solids. *Phys. Rev. B* **108**, 1–15 (2023).
54. J. Deslippe *et al*., BerkeleyGW: A massively parallel computer package for the calculation of the quasiparticle and optical properties of materials and nanostructures. *Comput. Phys. Commun.* **183**, 1269–1289 (2012).
55. S. Ponce, E. R. Margine, C. Verdi, F. Giustino, EPW: Electron–phonon coupling, transport and superconducting properties using maximally localized Wannier functions. *Comput. Phys. Commun.* **209**, 116–133 (2016).
56. A. Marini, Ab initio finite-temperature excitons. *Phys. Rev. Lett.* **101**, 1–4 (2008).
57. Z. Dai, C. Lian, J. Lafuente-Bartolome, F. Giustino, Theory of excitonic polarons: From models to first-principles calculations. *Phys. Rev. B* **109**, 1–19 (2024).
58. Z. Dai, C. Lian, J. Lafuente-Bartolome, F. Giustino, Excitonic polarons and self-trapped excitons from first-principles exciton–phonon couplings. *Phys. Rev. Lett.* **132**, 36902 (2024).
59. F. Bechstedt, K. Tenelsen, B. Adolph, R. Del Sole, Compensation of dynamical quasiparticle and vertex corrections in optical spectra. *Phys. Rev. Lett.* **78**, 1528–1531 (1997).
60. R. I. Biega, M. R. Filip, L. Leppert, J. B. Neaton, Chemically localized resonant excitons in silver-pnictogen halide double perovskites. *J. Phys. Chem. Lett.* **12**, 2057–2063 (2021).
61. M. E. Peskin, D. V. Schroeder, *An Introduction to Quantum Field Theory* (Francis Group, 1995).
62. K. T. Hecht, *Quantum Mechanics, Graduate Texts in Contemporary Physics* (Springer, 2012).
63. R. Perea-Causín, S. Brem, E. Malic, Phonon-assisted exciton dissociation in transition metal dichalcogenides. *Nanoscale* **13**, 1884–1892 (2021).
64. B. A. Lippmann, Rearrangement collisions. *Phys. Rev.* **102**, 264 (1956).
65. S. Sunakawa, On the theory of rearrangement collisions. *Progr. Theor. Phys.* **24**, 963 (1960).
66. T. B. Day, L. Rodberg, G. Snow, J. Sucher, Note on rearrangement collisions. *Phys. Rev.* **123**, 1051–1053 (1961).
67. C. J. N. Coveney, J. B. Haber, A. M. Alvertis, J. B. Neaton, M. R. Filip, Rearrangement collision theory of phonon-driven exciton dissociation. arXiv [Preprint] (2024). https://arxiv.org/abs/2405.13525 (Accessed 28 June 2024).
68. H. Fröhlich, Electrons in lattice fields. *Adv. Phys.* **3**, 325–361 (1954).
69. G. H. Wannier, The structure of electronic excitation levels in insulating crystals. *Phys. Rev.* **52**, 191–197 (1937).
70. N. F. Mott, Conduction in polar crystals. II. The conduction band and ultra-violet absorption of alkali-halide crystals. *Trans. Faraday Soc.* **34**, 500–506 (1938).
71. J. Voigt, F. Spiegelberg, M. Senoner, Band parameters of CdS and CdSe single crystals determined from optical exciton spectra. *Phys. Status Solidi B* **91**, 189–199 (1979).
72. M. A. Jakobson, V. D. Kagan, R. P. Seisyan, E. V. Goncharova, Optical properties of "pure" CdS and metal–insulator–semiconductor structures on CdS at electrical operation. *J. Cryst. Growth* **138**, 225–230 (1994).
73. T. S. Jeong, P. Y. Yu, T. S. Kim, Temperature dependence of the free excitons in a CdS single crystal. *J. Korean Phys. Soc.* **36**, 102–105 (2000).
74. K. Reimann, M. Steube, D. Fröhlich, S. J. Clarke, Exciton binding energies and band gaps in GaN bulk crystals. *J. Cryst. Growth* **189–190**, 652–655 (1998).
75. J. F. Muth *et al*., Absorption coefficient, energy gap, exciton binding energy, and recombination lifetime of GaN obtained from transmission measurements. *Appl. Phys. Lett.* **71**, 2572–2574 (1997).
76. Z. P. Yin, A. Kutepov, G. Kotliar, Correlation-enhanced electron–phonon coupling: Applications of GW and screened hybrid functional to bismuthates, chloronitrides, and other high-Tc superconductors. *Phys. Rev. X* **3**, 1–20 (2013).
77. B. Monserrat, Correlation effects on electron–phonon coupling in semiconductors: Many-body theory along thermal lines. *Phys. Rev. B* **93**, 100301(R) (2016).
78. J. Allerbeck, T. Deckert, L. Spitzner, D. Brida, Probing free-carrier and exciton dynamics in a bulk semiconductor with two-dimensional electronic spectroscopy. *Phys. Rev. B* **104**, L201202 (2021).
79. A. Jha *et al*., Direct observation of ultrafast exciton dissociation in lead iodide perovskite by 2D electronic spectroscopy. *ACS Photonics* **5**, 852–860 (2018).
80. E. H. Bogardus, H. B. Bebb, Bound-exciton, free-exciton, band-acceptor, donor–acceptor, and auger recombination in GaAs. *Phys. Rev.* **176**, 993–1002 (1968).
81. A. K. Viswanath, J. I. Lee, Exciton–phonon interactions, exciton binding energy, and their importance in the realization of room-temperature semiconductor lasers based on GaN. *Phys. Rev. B, Condens. Matter Mater. Phys.* **58**, 16333–16339 (1998).
82. J. J. Zhou, O. Hellman, M. Bernardi, Electron–phonon scattering in the presence of soft modes and electron mobility in $SrTiO_3$ perovskite from first principles. *Phys. Rev. Lett.* **121**, 226603 (2018).
83. C. Verdi, F. Giustino, Fröhlich electron–phonon vertex from first principles. *Phys. Rev. Lett.* **115**, 1–5 (2015).
84. L. Viña, S. Logothetidis, M. Cardona, Temperature dependence of the dielectric function of germanium. *Phys. Rev. B* **30**, 1979–1991 (1984).
85. S. Logothetidis, L. Via, M. Cardona, Temperature dependence of the dielectric function and the interband critical points of InSb. *Phys. Rev. B* **31**, 947–957 (1985).
86. L. Via, H. Höchst, M. Cardona, Dielectric function of α-Sn and its temperature dependence. *Phys. Rev. B* **31**, 958–967 (1985).
87. A. Miyata *et al*., Direct measurement of the exciton binding energy and effective masses for charge carriers in organic-inorganic tri-halide perovskites. *Nat. Phys.* **11**, 582–587 (2015).
88. C. L. Davies *et al*., Bimolecular recombination in methylammonium lead triiodide perovskite is an inverse absorption process. *Nat. Commun.* **9**, 1–9 (2018).
89. A. Miglio *et al*., Predominance of non-adiabatic effects in zero-point renormalization of the electronic band gap. *npj Comput. Mater.* **6**, 167 (2020).
90. J. B. Haber, D. Y. Qiu, F. H. da Jornada, J. B. Neaton, Maximally localized exciton Wannier functions for solids. *Phys. Rev. B* **108**, 125118 (2023).